OPTICAL/THERMAL ANALYSIS METHODOLOGY FOR A SPACE-QUALIFIABLE RTP FURNACE

D. Bugby and S. Dardarian
Swales & Associates, Inc.
Beltsville, Maryland

E. Cole
George Mason University
Fairfax, Virginia

Abstract

A methodology to predict the coupled optical/thermal performance of a reflective cavity heating system was developed and a laboratory test to verify the method was carried out. The procedure was utilized to design a rapid thermal processing (RTP) furnace for the ROMPS program which is a planned STS HH-G canister experiment involving robotics and material processing in microgravity. The laboratory test employed a tungsten-halogen reflector/lamp to heat thin, p-type silicon wafers. Measurement instrumentation consisted of 5-mil Pt/Pt-Rh thermocouples and an optical pyrometer. The predicted results, utilizing an optical ray-tracing program and a lumped-capacitance thermal analyzer, showed good agreement with the measured data for temperatures exceeding 1300 °C.

Introduction

The ROMPS (Robot-Operated Material Processing in Space) program involves integration of a robotics system and a high temperature rapid thermal processing (RTP) furnace in an STS HH-G canister. The ROMPS system consists primarily of a reflector/oven in which samples are annealed, racks for storing unprocessed or fully-processed samples, a robot to transport samples between the reflector/oven and rack, and associated controlling electronics. The objectives of the ROMPS program are to study post-deposition rheotaxy in microgravity and to demonstrate the viability of carrying out in-space material processing using robotics systems. The program is sponsored by the NASA Goddard Space Flight Center and involves a modeling effort by Swales & Associates, Inc. and an investigation of the application of the RTP system to candidate microgravity material processes by George Mason University.

The ROMPS furnace is an ellipsoid-shaped reflector with a tungsten-halogen lamp filament placed at one focus and the sample placed at the other focus. The system will heat 1 cm diameter, 10 micron thick (substrated) semiconductor films to prescribed temperatures in less than 10 seconds, maintain the samples at that temperature for periods ranging from several seconds to several minutes, and cool in approximately 2 minutes. Proposed test materials include silicon, cadmium telluride, gallium arsenide, and several others.

Due to the adverse effect on crystal growth of temperature gradients within samples during RTP, surface flux variations must be kept small. Ground-based single-wafer RTP systems can utilize several kilowatts to achieve the required radiative environment, while STS HH-G payloads are limited to 560 W. Thus, the design goal is a system which produces a relatively uniform flux over the sample surface with a minimum consumption of power.

To achieve this goal, a methodology to simulate the coupled optical/thermal phenomena within reflective cavity heaters was developed and was utilized to arrive at a preliminary ROMPS RTP furnace design. To verify the approach, a laboratory test was performed. This paper will describe the methodology, the laboratory test, the measured results, the model predictions, and the principal conclusions.

(NASA-CR-192254) OPTICAL/THERMAL ANALYSIS METHODOLOGY FOR A SPACE-QUALIFIABLE RTP FURNACE (Swales and Associates) 11 p

N93-19889

Unclas

G3/35 0147909

Analysis Methodology

The design of reflective heating systems such as that utilized in the ROMPS program is an iterative process. The required analytical tools include optical ray-tracing and lumped-capacitance thermal analysis computer codes. In this study, OPTICAD and SINDA are the respective analytical tools.[1,2]

The process is initiated by selecting a reflector shape and an actual tungsten-halogen bulb based on the size and power constraints of the particular application. The ray-tracing code is used to determine the fraction of emitted filament power which is incident on the sample surface and the spatial distribution of this power. The thermal analyzer is then utilized to determine the sample thermal response. If the performance is unacceptable, a new reflector and/or bulb is selected and the analysis is repeated.

An overview of the specific steps comprising the coupled optical/thermal analysis methodology is provided below. A detailed description of the procedure applied to the test configuration follows later in the paper.

Optical Modeling

As indicated, the first step in the procedure is the selection of a reflector geometry and a tungsten-filament bulb. This selection must include an analytical or numerical representation of the reflector shape (e.g., an ellipsoid), the reflector internal surface reflectivity (ρ), the geometry of the filament (l,w,t), and the filament operating temperature (T_f).

The second step is to set up an optical (ray-tracing) model of the system. The optical model includes the reflector, the filament (from which the rays emanate), and the sample (or target) which is to be heated. Depending on the capabilities of the ray-tracing code, an approximation to the desired reflector shape and the actual filament shape may have to be utilized. However, to obtain an accurate representation of the incident flux on the target surface, a three-dimensional distributed point source model of the filament is required.

Additional details to incorporate into the optical model are the non-transmissivity of the filament (the model must not allow reflected rays to pass through filament), non-ideal wall reflections (ray energy must be reduced by $(1-\rho)$ in each reflection), and target discretization with sufficient resolution to perform an adequate thermal response computation. Note that "target" and "sample" are used interchangeably throughout this paper.

Next, the ray-tracing calculation is carried out to obtain the fractional power distribution (ϕ_i) over the discretized target surface. In ray-tracing terms,

$$\phi_i = E_i / E_{tot} \qquad (1)$$

where E_i = energy of the rays striking target grid element (i) and E_{tot} is the total energy of the rays emitted from the filament. Due to non-ideal wall reflections, the energy of the rays is not necessarily equal to the number of rays.

Thermal Modeling

While the ray-tracing calculation provides the fractional distribution of power emitted by the filament incident on the target surface, it does not provide the magnitude of the filament emissive power. This quantity can be computed via the expression,

$$Q_f = \varepsilon_f A_f \sigma T_f^4 \qquad (2)$$

where A_f = effective surface area of the filament, ε_f = filament emissivity, σ = Stefan-Boltzmann constant, and T_f = filament operating temperature. The distribution of absorbed power over the target surface is thus given by,

$$Q_i = \alpha_s \phi_i Q_f \qquad (3)$$

where α_s = sample absorptivity to the incoming tungsten radiation spectrum. For silicon, α_s can vary markedly with temperature, wavelength, composition, and surface condition.

The next step in the procedure is to set up the (lumped-capacitance) thermal model of the target system. The thermal model must incorporate sample heating as defined by Equation (3), conduction within the sample, conductive heat loss from the sample to the surroundings, and sample heat loss by radiation. The radiation heat loss term can be approximated according the relation,

$$Q_{rad,i} = \gamma \varepsilon_s A_s \sigma (T_i^4 - T_o^4) \qquad (4)$$

where ε_s = sample emissivity, A_s = area of one face of the sample surface, γ = radiation re-emission parameter which typically varies between 1 and 2 for thin, flat targets, T_i = temperature of computational zone (i), and T_o = effective radiation sink temperature.

The final step is to compute the thermal response of the target system and assess whether the design is acceptable. In general, if the bulk steady-state temperature is acceptable but the gradient too large, defocusing the target away from the focal point will tend to even out the flux distribution over the sample surface. However, defocusing will also reduce the flux magnitude. If the bulk sample temperature is too low a different reflector shape, a different bulb, or both, are selected and the analysis is repeated. The basic governing thermal analysis equation is given below:

$$\{mc_p(dT/dt)\}_i = \alpha_s \phi_i Q_f - \Sigma G_c (T_i - T_j) - \gamma \varepsilon_s A_{s,i} \sigma (T_i^4 - T_o^4) \qquad (5)$$

To reduce computational effort, it is possible to estimate the average sample temperature using only the ray-tracing results. In the absence of conductive losses, the steady-state (radiation equilibrium) sample temperature can be estimated via the following relation,

$$T_{eq} = (\alpha_s \phi Q_f / \gamma A_s \varepsilon_s \sigma)^{.25} \qquad (6)$$

where $\phi = \Sigma \phi_i$. This equation can be utilized to perform a preliminary assessment of a given reflector design. The equation also provides some insight into optimal reflector design. Values of the various parameters indicated in the foregoing equations are listed in Table 1.

Table 1. Optical/Thermal Model Parameter Values and Their Definitions

Parameter	Definition (units)	Value Used
1. A_f	Effective filament area (mm^2)	44
2. T_f	Filament temperature (K)	3200
3. ε_f	Filament emissivity (@ 3200 K)	.35
4. α_s	Silicon absorptivity*	.71
5. ε_s	Silicon emissivity*	.71
6. ϕ	Fraction of filament emissive power incident on sample	.68
7. m	Mass of silicon wafer (kg)	2. E-4
8. c_p	Silicon heat capacity (J/kg K)	703
9. Q_f	Filament emissive power (W)	91.6
10. G_c	Conductive heat loss conductance (W/K)	.002
11. G_r	Radiative heat loss conductance (m^2) = $\varepsilon_s \gamma A_s$	1.6 E-4
12. γ	Re-radiation parameter	1.0
13. A_s	Sample single-face surface area (m^2)	2.25 E-4
14. T_o	Radiation sink temperature (K)	300

* Silicon absorptivity and emissivity assumed equal

Depending upon the configuration of the reflector and sample holder, the radiation re-emission parameter (γ) will typically have a value between 1 and 2. A value of 2 indicates the sample can freely radiate from both sides and a value of 1 indicates effective radiative "insulation" on the backface of the sample. By placing a reflective surface adjacent to the back-face of the sample, the radiative heat loss from the sample can be reduced. In a completely enclosed reflector with effective back-face radiative insulation, γ can potentially be less than unity. This result is due to energy emitted (or reflected) from the front face of the sample which reflects back onto the sample. Thus, to maximize sample temperature, the use of completely enclosed reflectors and backface radiative insulation is recommended.

To investigate the validity of the methodology outlined above, a laboratory experiment was performed. The test set-up was designed to enable the application of the aforementioned approach to a breadboard tungsten-halogen reflector-lamp system which is functionally similar to the ROMPS flight furnace design.

Experimental Procedures

The test fixture for positioning the lamp and sample is illustrated in Figure 1. The infrared heat source is a 150 W, 15 V Osram HLX 64635 tungsten-halogen reflector/lamp. This product is a combination of an internally gold-coated reflector and a tungsten-halogen bulb which can be purchased in this combined form. The lamp is mounted to three linear (micrometer) translation stages. The translation stages are attached perpendicular to one another providing the capability for fine adjustments to the x, y, or z position of the reflector/bulb and, thereby, precise sample-reflector positioning. The aforementioned equipment is bolted to a steel baseplate.

The test samples are bonded (using a high-temperature adhesive) to a fused-quartz sample holder with isolating "fingers" as shown in Figure 2. The sample holder is attached within a spherical bearing, the center of rotation of which is coincident with a point on, and at the center of, the sample surface. The spherical bearing is mounted in an aluminum fixture which is also bolted to the baseplate. The spherical bearing provides a means of rotating the sample to ensure sample-beam perpendicularity, without altering sample-source separation.

Samples are square 1.5 cm x 1.5 cm x 15.5 mil thick wafers of p-type silicon. Four 5-mil, S-type Pt/Pt-Rh thermocouples are adhesively bonded (using a high-temperature, conductive adhesive) directly to the back of the silicon samples. To simulate space flight vacuum, the entire apparatus is placed in a (12" x 12" I.D.) glass bell jar located at George Mason University. Vacuums of approximately 10^{-5} torr were utilized. A block diagram of the various experimental components is provided in Figure 3.

Relative Flux Map Measurement

To obtain a measurement of the flux distribution over the sample surface, a simple relative flux measurement device was constructed. A very small, thin piece of silicon (1.5 mm x 1.5 mm x 15.5 mil) was bonded to one of the 5-mil Pt/Pt-Rh thermocouples. The thermocouple was held in a ZERODUR sheath which was mounted in a hole at the center of a polished aluminum plate identical in outer shape to the quartz sample holder. The plate is mounted to the spherical bearing just as the sample holder is mounted. The flux measurement device is illustrated in Figure 4.

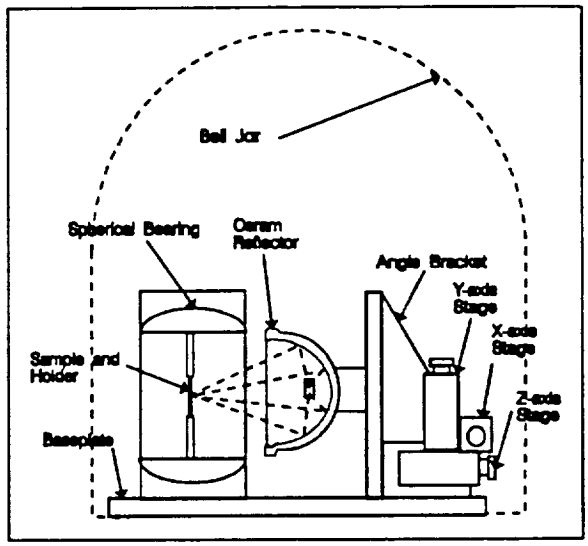

Figure 1. Sample Positioning/Heating Apparatus

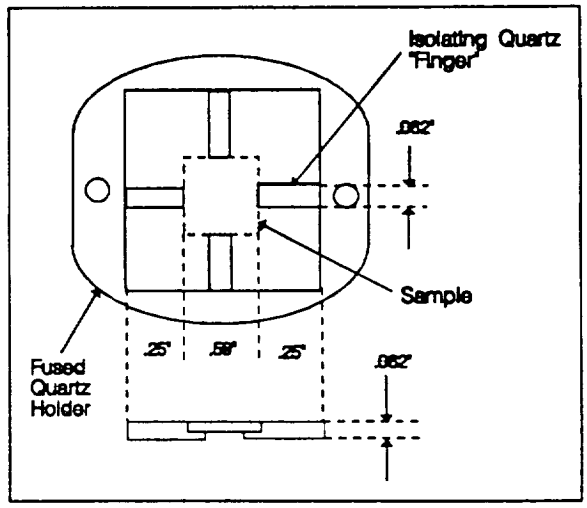

Figure 2. Sample Holder

The objective of the relative flux map measurement is to obtain experimental information which can validate the optical modeling portion of the coupled optical/thermal analysis methodology. In these tests, the

position of the silicon-thermocouple "detector" was held fixed. The lamp was then turned on. The x, y and z translation stages (the z-direction being perpendicular to the detector surface) are adjusted until the thermocouple reads a maximum temperature. This is the position of the focal point. By systematically varying the x and y positions of the reflector/lamp, while leaving z position fixed, the variation in the flux environment at the test sample surface (i.e., in the sample plane) can be ascertained.

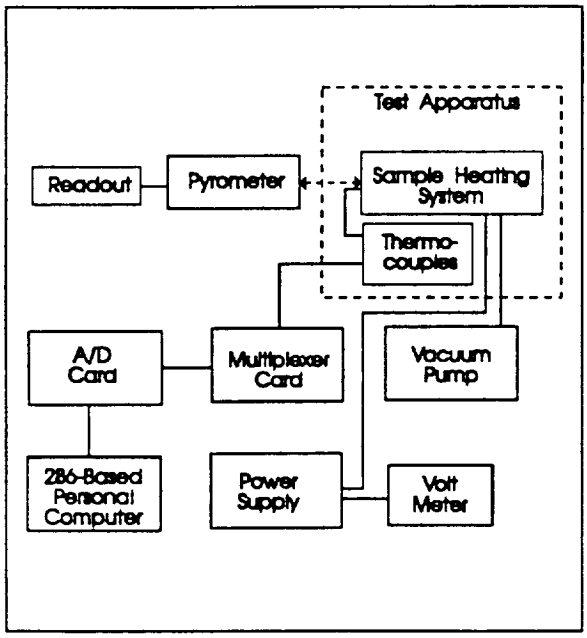

Figure 3. Experimental Components

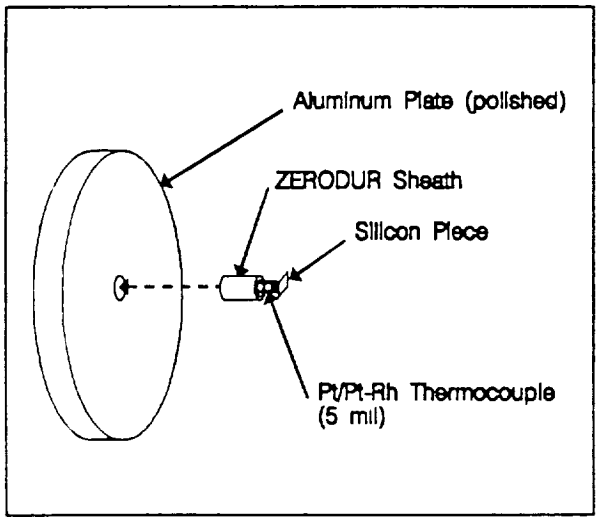

Figure 4. Relative Flux Map "Detector"

The method utilizes the assumption that the flux (q_i) incident at a location (i) in the test sample plane can be written as follows,

$$q_i = k\, T_i^4 \tag{7}$$

where k = constant and T_i = measured detector temperature. The value of the power incident on an area A_i nearby to location (i) over which q_i is relatively constant is given by,

$$P_i = A_i\, q_i \tag{8}$$

If the flux is mapped over a larger surface region S, where $S = \Sigma A_i$, the fraction of the total power (intercepted by S) which is incident on area A_i is given by,

$$\Phi_i = P_i / \Sigma P_i = A_i T_i^4 / \Sigma A_i T_i^4 \tag{9}$$

And, if the map locations (i) are chosen as the center points of identically-sized grid elements of size A (all $A_i = A$), the parameter Φ_i is given by

$$\Phi_i = T_i^4 / \Sigma T_i^4 \tag{10}$$

Comparing Equation (10) to Equation (1), it should be clear that the "measured" values of Φ_i should correspond with ray-tracing predictions as follows,

$$\Phi_i = E_i / \Sigma E_i \tag{11}$$

where E_i has been defined earlier. Equation (11) assumes that the discretization used in the ray-tracing calculation is identical to that used to derive the relative flux map. How well the left hand side of Equation (11) matches the right hand side is one measure of the validity of the optical model (note that $\Sigma E_i < E_{tot}$).

Steady-State Temperature Measurements

One objective of the steady-state temperature distribution measurements is to provide a means of calibrating one temperature measurement technique against another. As described above, the pyrometer could not be utilized to obtain transient temperature data due,

in part, to the low temperature transmissivity of silicon at the pyrometer operating wavelength. Another reason is the relatively slow response time (approximately .4-.5 sec) of the particular pyrometer used.

To make the steady-state pyrometer measurements, the emissivity of the silicon wafer was required. The available data indicate a value of .71 at temperatures over 1075 K for all sample thicknesses and over all wavelengths.[3] The procedure for obtaining the steady-state temperatures is straightforward. The samples were attached and mounted in the test fixture as described earlier. It should be noted that the pyrometer has a minimum spot size of .075" (1.91 mm) at a distance of 4" and is equipped with sighting optics for accurate spot positioning. The bell jar was placed over the apparatus and the vacuum pump was turned on reducing the pressure inside the jar to approximately 10^{-5} torr.

Using the sighting optics, the pyrometer was trained on a desired location on the silicon sample back surface. Then, the lamp was powered on. Within 15-20 seconds a constant digital temperature value was achieved. To obtain the temperature at several locations on the sample, the lamp power was cut off and the pyrometer was manually repositioned to a different location using the sighting optics. The power had to be cut off because one could not look into the sighting tube due to the brightness of the tungsten-halogen bulb.

Several tests were carried out to obtain steady-state thermocouple measurements. These tests included one transient test. In the steady-state tests, the real-time data acquisition capability of the a/d converter was not utilized. Data was obtained by (manually) making single a/d conversions. The procedure for performing the thermocouple measurement tests is essentially identical to that described above for the pyrometer.

Transient Temperature Measurements

The principal objective of the transient temperature measurements was to assess the overall accuracy of the coupled optical/thermal analysis methodology. The measurements also served as a means to refine the modeling. As will be seen, the transient temperature data obtained during the course of this experiment provided information on two important parameters in the analysis: the absorptivity of silicon (α_s) and the sample radiative re-emission parameter (γ).

In the transient test, the instant the power was turned on the a/d converter automatic data acquisition capability was enabled. One complicating factor is the transient power-up time of the tungsten-halogen lamp which is on the order of a few tenth's of a second. To account for this delay, a manually induced delay of less than one second was attempted following application of bulb power. The thermocouple data (time and temperature at each thermocouple location) was recorded to disk when temperature equilibrium was achieved.

Experimental Results and Analysis

In this section, the experimental results and the accompanying analytical predictions are presented. These include the measurements and analyses of the reflector geometry, the relative flux map, the steady-state temperature distribution, and the transient temperature distribution. Also included in a comparison against data provided by the reflector/lamp manufacturer and a thermal analysis which is useful in evaluating parameter sensitivities.

Reflector/Target Geometry

As described earlier, the first requirement to perform an optical ray-tracing simulation of a given system is an analytical or numerical representation of the reflector shape and the size and shape of the filament. Thus, to simulate the test configuration, the shape of the tungsten-halogen reflector and the size of its filament are required.

Two methods were utilized to determine the reflector shape. In each case, the reflector was assumed to be cylindrically symmetric. In the first method, the shape was precisely

measured on a numerically-controlled milling machine. The data was curve-fit to a eighth-order polynomial. The resulting polynomial is shown below (y,x are in inches),

$$y_1 = A\,x^2 + B\,x^4 + C\,x^6 + D\,x^8 \qquad (12)$$

where A=-0.770269, B=-1.324134, C=3.838006, and D = -4.335497. The value of x varies between -.84" and .84". The second method, which was the one actually utilized in the current investigation, approximated Equation (12) as an ellipse to accommodate ray-tracing code capabilities

Once the reflector shape is specified, additional information required to perform a ray-tracing calculation is the size of the target and the discretization required. The silicon test samples are square 1.5 cm x 1.5 cm wafers, thus the ray-tracing code target representation must be identical. To obtain sufficient resolution to compare with the flux map measurements and to perform adequate thermal response calculations, the surface of the wafer was divided into 25 square elements each of which are 3 mm on a side.

The filament in the Osram bulb is a tightly wrapped coil of 11-mil tungsten wire. The outer dimensions of the coil can be modeled as a 5 mm x 3 mm x 1 mm parallelepiped. The outer surface of the parallelepiped is divided into a grid of square surface elements. The center of mass of the parallelepiped is positioned at one focal point and light point sources are placed at the center of each surface grid element. Emission from each point source occurs over a hemispherical solid angle. An alternative approach is to construct a geometrically accurate model of the filament shape. Although the former method is utilized herein, the latter method obviates the need to estimate the effective filament surface area (A_f). In this case, there are 46 surface zones of size 1 mm x 1 mm. Figure 6 illustrates the filament model.

Relative Flux Map Predictions

Rays from each point source were emitted over a hemispherical (2π) solid angle with 20 equal increments in each angular direction for a total of 400 rays per point source. Thus, a total of 18,400 rays were emitted from the filament. The reflector wall was assumed to have a wall reflectivity of .95 and a maximum of 9 reflections were allowed before a ray was discarded. This maximum was obviously not achieved given the openness of the system.

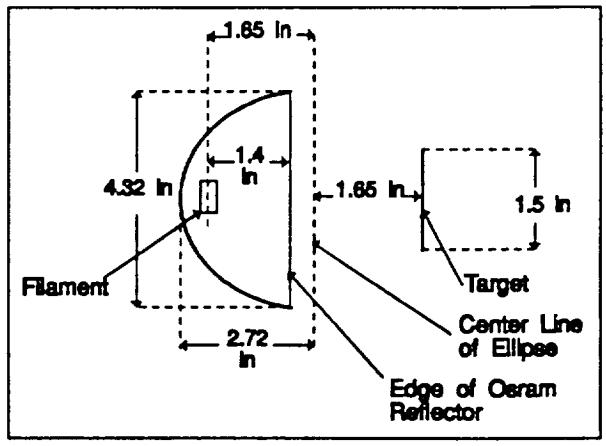

Figure 5. Experimental Reflector/Target Configuration

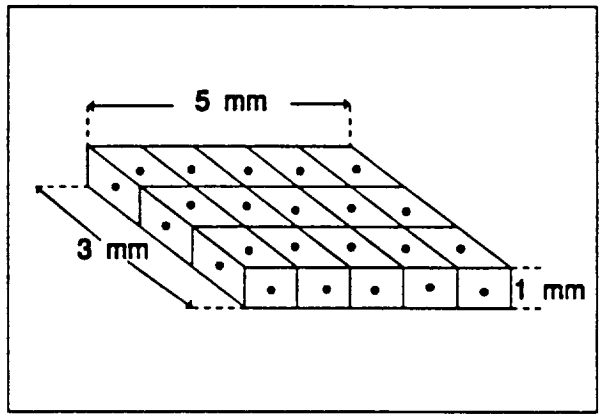

Figure 6. Filament Model Configuration

The ray-tracing results indicate that 13,184 rays struck the target with a total energy of ΣE_i = 12,524.7. Note that the ratio of these two numbers is simply the wall reflectivity (.95). The ray-tracing results for the values of each E_i are listed in Table 2. The values in the table have been normalized to a value of unity at the center. The x and y values correspond to the locations of the grid element centers. The measured flux distribution results are provided in Table 3.

Table 2. Predicted Relative Flux Distribution over the Sample Surface*

y\x mm	-6	-3	0	3	6
6	.046	.061	.042	.061	.046
3	.243	.569	.786	.569	.243
0	.414	.819	1.0	.819	.414
-3	.243	.569	.786	.569	.243
-6	.046	.061	.042	.061	.046

* values have been normalized to 1.0 at the center

Table 3. Measured Relative Flux Distribution over the Sample Surface*

y\x ,mm	-6	-3	0	3	6
6	.056	.135	.182	.170	.088
3	.154	.451	.611	.482	.226
0	.251	.615	1.0	.783	.312
-3	.216	.585	.713	.546	.225
-6	.119	.204	.315	.238	.104

* values have been normalized to 1.0 at the center

The results listed above indicate that the measured relative flux distribution has greater dispersion and non-uniformity than does the predicted distribution. This increased dispersion is probably due to a combination of lack of bulb/filament manufacturing uniformity, experimental error in accurately locating the spot center, and modeling approximation. The values at the center of the wafer are relatively close whereas the values around the wafer periphery differ moderately. The shape of the predicted distribution is not circularly symmetric, but is flattened out in the vertical direction and stretched out in the horizontal direction. While the measured distribution exhibits a greater degree of circular symmetry, the flattening effect is also observed.

The flattening effect is due, in part, to the orientation of the filament relative to the target. The longer dimension of the filament (5 mm) is oriented along the target's horizontal axis while the shorter dimension (3 mm) is oriented perpendicular to the target. The greater vertical dispersion seen in the measured distribution is possibly due to the difference between the approximate shape of the modeled reflector and its actual shape.

Post-test observations of a preliminary test sample revealed a 1 cm diameter circular-shaped region on the front and back faces of the heated wafer where oxidation had occurred. Based on the approximate time of heating, the oxygen partial pressure, and the coloration pattern of the oxidation zone, it is estimated that surface temperatures of at least 1000 °C at the zone outer periphery were achieved. These results serve as additional confirmation of the measured flux (and temperature) data and predictions.

Steady-State Temperature Predictions

The locations on the silicon wafers where pyrometer and thermocouple measurements were taken are indicated in Figure 7. Thermocouples were labeled T0, T4, T1, and T3 in order of increasing distance from the center of the sample. In this figure, the view of the silicon is from the back or unheated side of the wafer. The measured and predicted steady-state wafer temperature distributions are listed in Figures 8 - 10. Figure 8 provides the average pyrometer measurements from several tests, Figure 9 provides the average thermocouple measurements from several tests, and Figure 10 depicts the predicted steady-state results. The temperature measurements were reasonably repeatable from test to test.

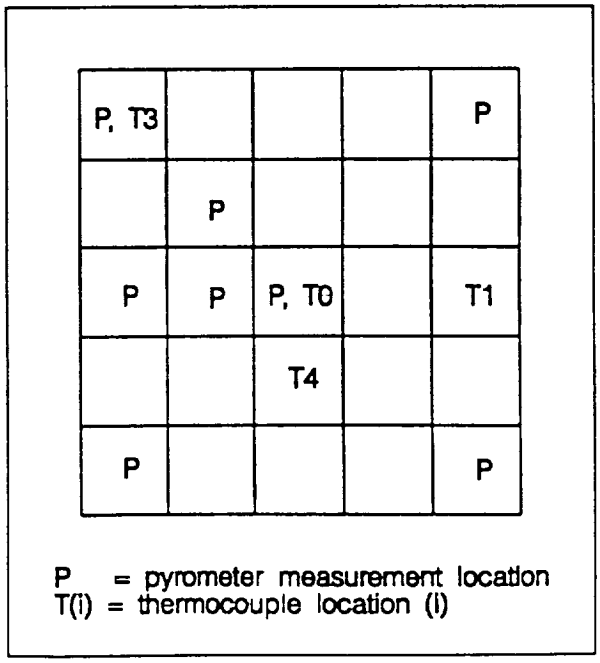

Figure 7. Pyrometer and Thermocouple Measurement Locations

The pyrometer measurements were increased by 80 °C due to the presence of the bell jar. This value held constant over the temperature range of interest and was measured by running in-air tests and recording the temperature drop upon placement of the bell jar between the pyrometer and sample.

For thermal modeling purposes, the silicon wafers were divided into 25 equally sized, square computational zones. Variations across the thickness of the wafer were assumed to be negligible. The fused-quartz sample holder was also included in the thermal model as was re-radiation to a room temperature sink in the manner indicated in Equation (5). Computation of silicon wafer thermal response included a finite (and temperature dependent) silicon thermal conductivity as denoted below,

$$k_{Si} = 2.99 \times 10^4 / (T\text{-}99) \qquad (14)$$

where the temperature values in Equation (14) are in K.[4] Using the parameter values listed in Table 1 and the flux map derived from the ray-tracing calculations (Table 2), the transient thermal response of the wafers was calculated and these results, along with the experimental measurements, are shown in Figures 11 and 12.

1030				1050
	1096			
1118	1221	1315		
1069				1012

Figure 8. Pyrometer Steady-State Temperature Measurements

Transient Temperature Predictions

The thermal conductivity and heat capacity of silicon are reasonably well-defined functions of temperature over the temperature range of interest here.[4] Therefore, to correctly predict the transient thermal response of heated silicon wafers, the following computations are required. First, the rate that energy is absorbed by the silicon at each location on the surface of the sample must be correctly predicted. These rates are required in order to match the initial temperature rise rate before radiative losses become important. Second, to achieve the correct steady-state temperature, not only is the rate that energy is absorbed by the silicon at each surface location required, but so is the rate that radiative energy is lost.

876				
		1359		1031
		1224		

Figure 9. Thermocouple Steady-State Temperature Measurements

1085	1110	1108	1110	1085
1161	1238	1281	1238	1161
1190	1302	1354	1302	1190
1161	1238	1281	1238	1161
1085	1110	1108	1110	1085

Figure 10. Predicted Steady-State Temperature Distribution

To carry out the first calculation, assuming the surface relative flux distribution is known (and is valid), one must know the filament output (Q_f), the fraction of the filament output which intercepts each surface region (ϕ_i),

the surface absorptivity (α_s), and the surface emissivity (ε_s), at all times during the calculation. To carry out the second calculation, one must also know the radiative environment surrounding the re-emitting wafer. Because of uncertainty in the low-to-moderate temperature radiative properties of silicon (from 20 - 650 °C), as well as difficulties in modeling the radiative environment surrounding the wafer, the experimental data was used to refine the model.

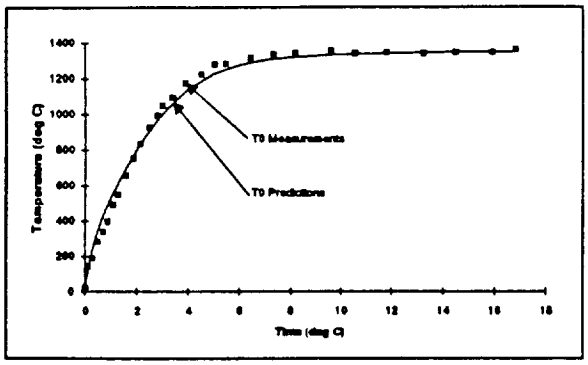

Figure 11. Comparison of Measurements and Predictions at Thermocouple Location T0

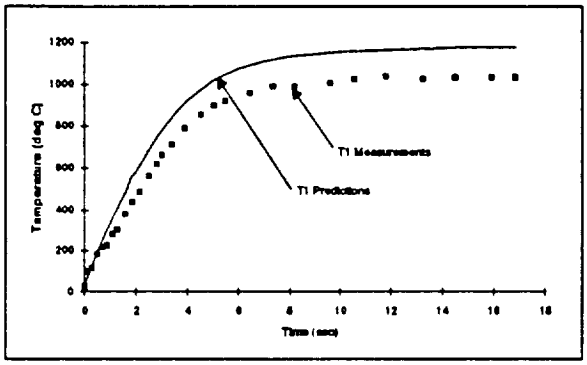

Figure 12. Comparison of Measurements and Predictions at Thermocouple Location T1

It was found that the initial rate of temperature rise was reasonably well predicted if the high temperature emissivity of silicon was used as the absorptivity value as well as the emissivity value (i.e., $\alpha_S=\varepsilon_S=.71$) throughout the calculation. In addition, it was found that the steady-state temperatures were reasonably well predicted if the re-radiation parameter γ (defined as the effective re-radiation area divided by the irradiated area) was assigned a value of unity rather than a seemingly more logical value between 1 and 2. The rationale for this approach is provided below.

Since there is uncertainty in the filament emissive power (Q_f) and the power fraction (ϕ), and since the product $\alpha_S\phi Q_f$ defines the initial temperature rise rate and the ratio $\alpha_S\phi Q_f/\gamma\varepsilon_S$ defines the steady-state wafer temperature, readjustment of α_S, ε_S, ϕ, Q_f, and/or γ might have been attempted. However, γ was deemed the most uncertain parameter of the five in question, and readjustment of one parameter rather than several was a preferable course of action. In future ROMPS testing and analysis, these uncertainties will be investigated.

With the foregoing in mind, the results depicted in Figures 11-12 indicate a favorable agreement between the predictions and the measured data. The center thermocouple (T0) follows the data almost perfectly over the duration of the test. The comparison with the edge thermocouple (T1) is less favorable. The wafer edge temperature measurement is lower than the prediction in initial (temperature rise) rate and in the steady-state temperature achieved. Thermocouple locations T3 and T4, while not shown, indicate transient responses that fall between T0 and T1. Overall, the data and predictions indicate initial temperature rise rates of 150-400 °C/sec, times to steady-state of 5-10 seconds, and steady-state temperatures between 900 and 1350 °C.

Summary and Conclusions

A methodology for predicting the coupled optical/thermal performance of reflective cavity heaters was developed. To verify the approach, a laboratory test was performed involving the heating of p-type silicon wafers. Measurements of relative flux and wafer surface temperatures were compared to predictions.

The predicted relative flux distribution matched the measured distribution near the center of the wafer, but differed near the wafer periphery. The predicted distribution was oval-shaped (flattened out in the wafer vertical

direction and stretched out in the wafer horizontal direction), while the measured distribution appeared to be more circular. Transient and steady-state temperature measurements compared well with the predictions near the wafer center, but deviated moderately near the wafer periphery. Pyrometer measurements were closer to predictions near the wafer corners than were the thermocouple results. The reason for this difference is not clear.

Due to the uncertainty in the radiative re-emission factor (γ), its pre-test value was readjusted to produce a better match with the data. In the predicted results, a close comparison was obtained by setting $\alpha_s=\varepsilon_s=.71$ (which is the high-temperature emissivity of unoxidized silicon) and $\gamma=1$ (which is the value for one-sided radiative re-emission).

Overall, the predictions showed favorable agreement with the measurements. Several areas of analytical and experimental uncertainty exist, however. Future testing and analysis are planned using a machined reflector where the reflector shape and filament position can be closely controlled. In this planned test, thermocouple instrumentation and pyrometer calibration will be utilized and an absolute surface flux map will be measured.

References

(1) OPTICAD (vers. 2.9) User's Manual, Opticomp Corp., Sante Fe, NM (1990).

(2) Gaske, J.D., *Systems Integrated Numerical Differencing Analyzer* (SINDA), Network Analysis Associates, Inc. (1987).

(3) Touloukian, Y.S. and Ho, C.Y. (editors), *Thermophysical Properties of Selected Aerospace Materials - Part I: Thermal Radiative Properties*, TEPIAC/CINDAS, Purdue University, West Lafayette, IN (1976).

(4) Grigoropoulous, C.P., Dutcher, W.E., Jr., and Emery, A.F., "Experimental and Computational Analysis of Laser Melting of Thin Silicon Films," *J. Heat Transfer*, Vol. 113, p.p. 21-29 (Feb. 1991).

(5) Osram Corp., *Light for Cine Projection Technology and Science*, NY (1987).

(6) Edwards, D.K., Denny, V.E., and Mills, A.F., *Transfer Processes*, 2nd Ed., McGraw-Hill, NY (1979).

(7) Roozeboom, F. and Parekh, N., "Rapid Thermal Processing Systems: A Review with Emphasis on Temperature Control," *J. Vac. Sci. Technol.*, Vol. 8, No. 6, p.p. 1249-1259, (Dec. 1990).